Competing Gas-Phase Substitution and Elimination Reactions of Gemini Surfactants with Anionic Counterions by Mass Spectrometry. Density Functional Theory Correlations with Their Bolaform Halide Salt Models†

Carole Aimé,‡ Benoit Plet,§ Sabine Manet,⊥ Jean-Marie Schmitter,¶ Ivan Huc,△ and Reiko Oda*

Institut Européen de Chimie et Biologie, University of Bordeaux, UMR 5248 CNRS U-Bx1, ENITAB, 2 rue Robert Escarpit, 33607 Pessac, France

Ronald R. Sauers* and Laurence S. Romsted*

Department of Chemistry and Chemical Biology, Rutgers, The State University of New Jersey, New Brunswick, New Jersey 08903

Received: April 1, 2008; Revised Manuscript Received: September 17, 2008

Understanding ion specific effects on the solution properties of association colloids is a major unsolved problem, and we are studying the chemistry of gemini surfactants in the gas-phase by mass spectrometry and density functional theory (DFT) to probe ion specific effects in the absence of water. Products from gas-phase fragmentation chemistry of dication−monoanion pairs, $M^{2+}X^-$, of $C_{16}H_{33}(CH_3)_2N^+$-$(CH_2)_n$-$^+N(CH_3)_2C_{16}H_{33}\cdot 2X^-$ gemini surfactants were determined by using sequential collision induced dissociation mass spectrometry. The spacer length "*n*" was systematically varied ($n = 2$, 3, 4, and 6) for each counterion investigated ($X^- = F^-$, Br^-, Cl^-, I^-, NO_3^-, $CF_3CO_2^-$, and PF_6^-). The $M^{2+}X^-$ pairs fragment into monocationic products from competing E2 and S_N2 pathways that are readily quantified by tandem MS. The dominant reaction pathway depends on dication and anion structure because it switches from E2 to S_N2 with decreasing anion basicity and increasing spacer length. For spacer lengths $n = 4$ and 6, the major S_N2 product shifts from attack at methylene to methyl on the quaternary ammonium group. DFT calculations of gemini headgroup model bolaform salts, $CH_3(CH_3)_2N^+$-$(CH_2)_n$-$^+N(CH_3)_2CH_3\cdot 2X^-$ ($X^- = F^-$, Cl^-, Br^-, and I^-, $n = 2-4$), primarily of activation enthalpies, $\Delta H^‡$, but also of free energies and entropies for the dication−monoanion pairs, $M^{2+}X^-$, provide qualitative explanations for the MS structure−reactivity patterns. $\Delta H^‡$ values for S_N2 reactions are independent of X^- type and spacer length, while E2 reactions show a significant increase in $\Delta H^‡$ with decreasing anion basicity and a modest increase with spacer length. Comparisons with the $\Delta H^‡$ values of model $CH_3CH_2(CH_3)_3N^+X^-$ halides show that the second charge on the dicationic ion pairs does not significantly affect $\Delta H^‡$ and that the change in distance between the nucleophile and leaving group in the ground and transition states structures in S_N2 reactions is approximately constant indicating that $\Delta H^‡$ is governed primarily by electrostatic interactions.

Introduction

Studies of structure−reactivity relations of dimeric salts, both anionic and cationic, and their counterions, are providing new insight into the factors controlling ionic interactions and chemical reactivity in the absence of solvent in the gas-phase.[1] Concurrently and independently, research on gemini (twin tail/twin headgroup or dimeric) surfactants is providing new insight into headgroup and counterion type effects on the forces controlling their self-assembly in aqueous solutions.[2−4] Combining gas phase and solution studies should eventually provide a comprehensive understanding of ion specific effects.

Here we report the results of a combined mass spectrometry (MS) and density functional theory (DFT) study of gemini spacer length and specific anion effects on competing substitution and elimination reactions in the gas-phase. This research is part of a larger project aimed at understanding ion specific headgroup, counterion, and hydration effects on the balance of forces controlling the self-assembly and morphological properties of gemini surfactants and their chemistry in solution.[2] Specific ion effects have been widely studied since Hofmeister's seminal paper in 1888[3−10] in a variety of systems including proteins, membranes, polyelectrolytes, and ion selective electrodes. Ion specific effects play a key role in determining the bulk properties of ionic association colloids such as micelles. Indeed, the critical micellar concentration (cmc),[11] Krafft temperature,[11−13] fractional charge of the micellar surface (ionization degree, α),[11,13,14] number of surfactant monomers per micelle (aggregation number),[15] and the phase separation temperature (cloud point)[16] all depend on headgroup structure, counterion type, and concentration. However, consensus is still absent on the mechanism by which specific ions exert their influence.[3]

† Part of the "Janos H. Fendler Memorial Issue".

* To whom correspondence should be addressed. E-mail: (R.O.) r.oda@iecb.u-bordeaux.fr; (R.R.S.) sauers@rutchem.rutgers.edu; (L.S.R.) romsted@rutchem.rutgers.edu.

‡ E-mail address: c.aime@mail.cstm.kyushu-u.ac.jp.

§ E-mail address: benoit.plet@covalx.com.

⊥ E-mail address: sabine.manet@gmail.com.

¶ E-mail address: jm.schmitter@iecb.u-bordeaux.fr.

△ E-mail address: i.huc@iecb.u-bordeaux.fr.

10.1021/jp802801r CCC: $40.75
Published on Web 11/13/2008

SCHEME 1

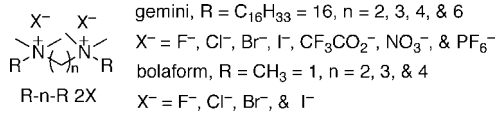

Gemini surfactants assemble spontaneously in aqueous solution into a variety of aggregate structures, for example, spherical, rodlike, lamellar, ribbons, and vesicular aggregates[17] that depend on the lengths of the hydrocarbon tails and headgroup structure.[18,19] Specific counterions have been used to induce morphological transitions (sphere-to-rod;[20] submicrometric vesicle-to-giant liposome;[21] and vesicle-to-micelle[22]) and to tune supramolecular morphologies (chiral structures from chiral counterions[23]).

Organic reactions in the gas-phase have been extensively reviewed,[1,24−26] as have competitive fragmentation pathways.[27−32] Tertiary amine leaving groups in a family of alkanediyl-α,ω-bis(dimethylalkylammonium dianions) surfactants (gemini) and bis(trimethyl)-α,ω-alkanediammonium salts (also called bolaform salts, as in an Argentinean gaucho's bola), Scheme 1, have been used to investigate S_N2 and E2 reaction mechanisms in the gas phase[27,33−37] and in solution.[38,39] The gas-phase chemistry of dication−monoanion pairs, $M^{2+}X^-$, is of particular interest because the fragmentations of these ion pairs are unimolecular analogs of competing bimolecular nucleophilic substitution, S_N2, and elimination, E2, reactions, and we will refer to these unimolecular fragmentations as such. The ion pairs fragment relatively easily, and the product distributions permit comparison of dication structure and anion type effects on competing nucleophilic substitution and elimination pathways from a single complex. Our MS experiments are similar to Gronert's "ionic platform approach"[28] except that our reactants are of the opposite polarity; our nucleophiles are monoanions and the electrophiles are dications. Both pathways lead to monocationic quaternary ammonium products that are observable by mass spectrometry (see Schemes 2 and 3 in Results). Gemini fragmentations as a function of changing spacer type and aliphatic chain lengths,[35,36] or/and counterion type (Br^-, I^-, Cl^- and AcO^-)[40] have been also reported, but these results have not been compared with calculated activation enthalpies.

Here we report competitive product yields from the gas-phase fragmentation of dication−monoanion pairs, $M^{2+}X^-$, obtained from R-*n*-R 2X ($R = 16$) salts, Scheme 1, using combinations of spacer lengths and counteranion types. The number of methylenes varied between $n = 2$ and 6 and the counteranions cover a significant range of basicities and nucleophilicities. Tandem mass spectrometry was used to isolate and fragment the $M^{2+}X^-$ pairs. The internal energy was increased by collision-induced dissociation (CID)[41] in an ion trap mass spectrometer.[42] The energy resolved mass spectrometry (ERMS) method was used to sequentially increase the energy and record the disappearance of $M^{2+}X^-$ along with the appearance of the resulting products as a function of increasing energy. DFT calculations were used to estimate the enthalpies, free energies, and entropies of activation for bolaform salts, which are models for the gemini headgroups, and halide counterions (Scheme 1, R = 1, $n = 2-4$, $X^- = F^-$, Cl^-, Br^-, I^-). Although the double-well potential energy surface introduced by Brauman[43] is the standard for interpreting gas-phase reactions, because the $M^{2+}X^-$ pairs are much more stable than the free ions, our DFT calculations are focused on the relative energies of the ion pairs as ground-state structures and their corresponding S_N2 and E2 (syn and anti) transition structures.

Experimental Section

Synthesis. 16-*n*-16 2X, X = Br, gemini surfactants were synthesized and recrystallized as previously reported.[44] 16-*n*-16 2X surfactants with other counterions were prepared from the bromide salts by two different methods depending on counterion type. All other reagents were of the highest purity available and used without further purification.

Preparation of Gemini with $F^-$and $CH_3CO_2^-$ (Ac^-) Counterions. 16-*n*-16 2Ac, which is used as an intermediate in the preparations of gemini with other counterions (see below), and 16-*n*-16 2F were synthesized from their respective silver salts. In a typical procedure, 16-*n*-16 2Br (1 g) was dissolved in 30 mL MeOH and stirred with 2.2 mol equivalents of AgAc or AgF for 15 min. The black precipitate of AgBr was removed by filtration through Celite and the MeOH was removed by using a rotoevaporator. The remaining white powder was recrystallized by dissolution in a small amount of MeOH and precipitation with acetone for 16-*n*-16 2Ac and diethyl ether for 16-*n*-16 2F. Yields exceeded 90%.

Surfactant purity was checked by a general procedure. AgAc was added to the gemini dissolved in MeOH. If a black precipitate indicating the presence of Br^- was observed, a small amount of AgAc or AgF was added, and the filtration and isolation procedure described above was repeated. Excess AgF and AgAc were removed by filtration through Celite. We note that 16-*n*-16 2F is prone to fragmentation (see below), particularly 16-2-16 2F, which started decomposing during synthesis. This problem prevented determining product yields by MS with spacer lengths 2 and 3 for F^- counterions.

Preparation of Gemini with $X^- = Cl^-$, NO_3^-, PF_6^-, $CF_3CO_2^-$, and I^- Counterions. In a typical procedure, 16-*n*-16 2Ac (100 mg) was dissolved in 15 mL of MeOH, 2.2 equivalents of HX, the acid carrying the needed surfactant counterion, was added, and the solution was stirred for 15 min while the MeOH and acetic acid were removed by using a rotoevaporator. 16-*n*-16 2X was dissolved in a small amount of MeOH (ca. 1 mL) then precipitated by the addition of acetone or diethyl ether. The remaining excess HX was removed during filtration. The sample was washed several times with the precipitating solvent to ensure that surfactants contained no remaining acid. Yields were at least 85%. The signal for the acetate methyl group, $\delta = 1.9$ ppm, was absent in the ^1H NMR spectra of each surfactant showing that at least 95% of the Ac^- was replaced.

Mass Spectrometry. Experiments were performed on an LCQ Advantage ion trap mass spectrometer (ThermoFinnigan, San Jose, CA) fitted with an orthogonal electrospray ionization (ESI) source. Room temperature was kept constant at 295 ± 1 K; ambient temperature inside the instrument was measured at 300.0 ± 0.7 K, close to the value reported for the same instrument setup used by Gabelica and others.[45−47] In addition, as described below, by reporting MS product yields as function of normalized collision energies, %NCE, the reactions of all ions are normalized to the same effective temperature in the MS experiments because %NCE includes an empirical correction for the *m*/*z* dependence of the fragmentation efficiency and because all the ions have essentially the same dependence of the effective temperature on the activation amplitude.[45] Finally, all MS experimental parameters were carefully kept constant to ensure minimum temperature variation (see below).

Spectra were obtained in positive ion mode over the 150−2000 *m*/*z* range with a number of parameters held constant: the spray voltage at 4.5 kV; the capillary temperature at 130 °C at a capillary voltage of 10 V; a tube lens offset of 0 V; a

SCHEME 2: S_N2 Reaction Products

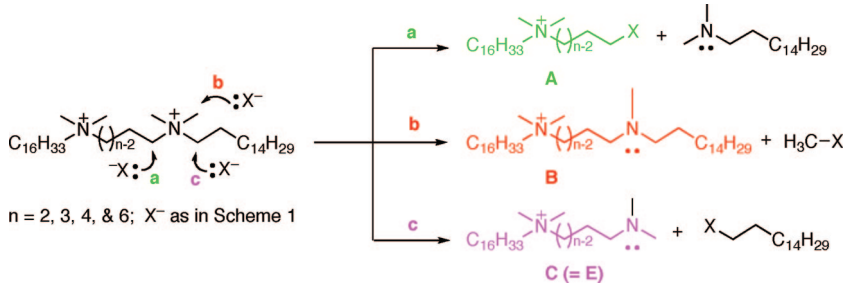

SCHEME 3: E2 Reaction Products from Both Syn and Anti Pathways[a]

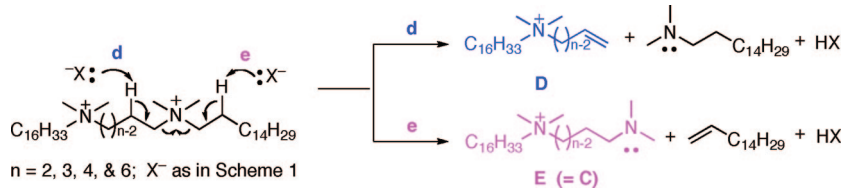

[a] Cationic product from pathway e is equivalent to that from pathway c in Scheme 2.

constant flow rate of N_2 for ion desolvation; solvent composition; and a flow rate of 300 μL/h for sample infusion using a syringe pump (Kd Scientific, Holliston, MA). Tandem mass spectrometry was performed in the ion trap by collision induced dissociation (CID) with helium gas buffer at 0.1 Pa.[41]

In all ERMS experiments, a 6 Th (m/z) isolation width was used for precursor ions, $M^{2+}X^-$, and the q_z value was constant at 0.25. Precursor ions were activated with increasing percentages of normalized collision energy (%NCE). %NCE is an experimental correction of the m/z dependence of fragmentation efficiency.[45,48]

$$\%\mathrm{NCE} = V_{\mathrm{pp}} \times \frac{30}{[0.4 + 0.002(m/z)]} \qquad (1)$$

where V_{pp} (in volts) is the peak-to-peak amplitude of the effective voltage applied to the end-cap electrode during resonance excitation.

Data acquisition was achieved in 140 steps of 0.2%NCE for 30 ms each. Two microscans of 200 msec were used per scan. Xcalibur, version 1.5 (ThermoFinnigan), was used for data acquisition. Precursor ions were isolated and monitored using their exact masses. The raw ion current (IC^{raw}) was normalized by dividing the measured ion current by the pseudo total ion current that was the sum of the ion currents of the 6 major ions that are identified products from the fragmentation reactions.[49]

$$\mathrm{IC}^{\mathrm{final}} = \frac{\mathrm{IC}^{\mathrm{raw}}}{\sum_{i=1}^{6} \mathrm{IC}_i} \qquad (2)$$

Data Analysis. Each ERMS experiment for a particular gemini was run in triplicate with very small average variation for the three data sets (~0.01%). Each data set was fitted using a Boltzmann sigmoidal function[49] available in Microcal Origin (Microcal Software, Inc. Northampton, MA) to give plots of the relative abundance of the precursor complex ($M^{2+}X^-$) versus applied %NCE. The fits of the three data sets were averaged and used to obtain the %NCE at which half of the $M^{2+}X^-$ pair had fragmented to products: $\%CE_{50}$. Prior control experiment on the LCQ Advantage MS showed that $\%CE_{50}$ values do not change significantly, ca. 1%, over many days. Therefore, we did not use a correction factor for long-term variations of $\%CE_{50}$. However, the $\%CE_{50}$ values were corrected for the degrees-of-freedom of the $M^{2+}X^-$ pair.[50] Data sets for the relative abundance of E2 and S_N2 products versus %NCE were smoothed using FFT-filtering available in Microcal Origin over 20 data points. The yields of product ions at $\%CE_0$, that is, at complete fragmentation of the $M^{2+}X^-$ precursor complex, were determined graphically, averaging relative peak intensity above a certain %NCE in the plateau region or in a few cases, where the highest relative abundance is obtained (see Figure 2 in Results).

Computational Methodology. All structures were fully optimized by analytical gradient methods using the Gaussian03 suite[51] and DFT calculations at the 6-31+G(d) level, the exchange functional of Becke[52,53] and the correlation functional of Lee, Yang, and Parr.[54] For calculations with Br^- and I^-, we used LANL2DZ effective core potentials.[55] Because the effects of addition of diffuse s, p functions and d polarization functions to LANL2DZ effective core potentials were relatively small (1.5 kcal/mol), we chose not to use these extra basis functions.[56] Vibrational analyses established the nature of all stationary points as either energy minima (no imaginary frequencies) or first order saddle points (one imaginary frequency). Animation of the imaginary frequencies for the various reaction types confirmed the nature, that is, substitution versus elimination, of the computed transition structures. The expected products from the substitution and elimination reactions of the fluoro system with spacer = 2 were confirmed by intrinsic reaction coordinate calculations. Reported enthalpy and free energy data have been corrected for zero point energy and thermal effects at 298.15 K. No attempts were made to study the systems with $n = 6$ or with PF_6^-, $CF_3CO_2^-$, and NO_3^- ions due to expected computer and other limitations, for example, the significant convergence problems that we encountered with initial attempts with NO_3^- ions.

Starting geometries for the lowest energy ground structures of the free bolaform dications were assumed to have conformations with all-trans methylene chains. This maintained the two positive centers at maximum separation and kept the repulsive forces at a minimum. Different conformations of the 1-n-$1^{2+}X^-$

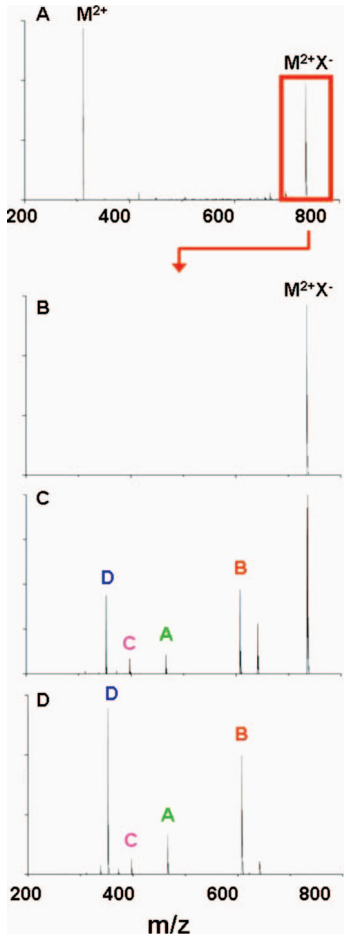

Figure 1. (A) ESI+ mass spectrum of 16-6-16 $2CF_3CO_2$. The peaks at $m/z = 311.3$ and at $m/z = 735.7$ are, respectively, the masses of the M^{2+} and $M^{2+}X^-$. The red box shows the isolation of the $M^{2+}X^-$ peak in (B) for MS/MS at CE_{100}. (C) Products from fragmentation of 16-6-16 $2CF_3CO_2$ upon MS/MS of $M^{2+}X^-$ at CE_{50} and (D) at CE_0.

cation pairs were explored to locate global minima. Ultimately, the lowest energy structures placed the anions centered between the two trimethylammoniun groups, thus optimizing electrostatic interactions. Initial transition structures for E2 and S_N2 reactions were optimized with minimal structural changes from lowest energy $M^{2+}X^-$ pair.

The importance of basis set superposition errors (BSSE) was evaluated by using the counterpoise method[57] for the ion pairs and the three reaction types: syn- and anti-E2 eliminations and S_N2 substitutions. We found that corrections were small for the $\Delta H^{\ddagger}$ values of the fragmentation reactions, typically <1 kcal mol^{-1}. However, the corrections for ion-pair formation were more significant for Br^- and I^- and the BSSE corrected values for all complexes are reported in Table 2 (see Results).

E2 and S_N2 reactions for ethyltrimethylammonium halides, M^+X^-, pairs were optimized at the B3LYP/6-31+G(d) level to assess the effects of the second charged center on these reactions. The reactivity trends were accurately reproduced with a few minor exceptions. Use of a larger basis set, B3LYP/6-311+G(d), had a relatively minor effect on the results, <1 kcal/mol. The significance of electron correlation effects was checked by comparison of these DFT results with MP2/6-31+G(d) calculations on the S_N2 and E2 reactions of the related M^+X^- pairs. Although the computed DFT activation enthalpies of these reactions are significantly smaller than the MP2 energies, numerical trends of enthalpies of activation, $\Delta H^{\ddagger}$, for both the S_N2 and E2 reactions are essentially the same for all M^+X^- pairs (see Table S5 of the Supporting Information). Expansion of the basis set for the fluoro M^+X^- and iodo M^+X^- pairs to MP2/6-311+G(d) had virtually no effect (<0.4 kcal/mol) on the energetics of the elimination and substitution reactions.

TABLE 1: Measured and Normalized Yields for Competing S_N2 and E2 Pathways[a]

X^-	n	Meas $\%A$	Meas $\%B$	Meas $\%D$	Norm $\%(A + B)$[b] S_N2 Products	Norm $\%D$[c] E2 Product
F^-	4	0	0	100	0	100
	6	0	0	100	0	100
Cl^-	2	20.4	0	79.6	20.4	79.6
	3	13.4	0	86.6	13.4	86.6
	4	96.4	0	3.6	96.4	3.6
	6	40.3	49.7	0	100	0
Br^-	2	77.3	6.7	10.3	89.0	11.0
	3	66.4	15.6	14.1	85.3	14.7
	4	86.8	4.3	0.2	99.8	0.2
	6	30.2	61.9	0.2	99.8	0.2
I^-	2	78.7	14	0	100	0
	3	87.8	10.1	0.1	99.9	0.1
	4	94.0	5.1	0.2	99.8	0.2
	6	33.7	60.8	0	100	0
$CF_3CO_2^-$	2	0.1	3.1	96.2	3.2	96.8
	3	0.3	0.9	98.7	1.2	98.8
	4	52.2	1.1	40.5	56.8	43.2
	6	11.1	34.3	50.5	47.3	52.7
NO_3^-	2	0.4	1.3	97.7	1.7	98.3
	3	0.2	0.5	99.2	0.7	99.3
	4	57.8	1.0	40.2	59.4	40.6
	6	18.2	60.8	5.3	93.7	6.29
PF_6^-	2	0	0	100	0	100
	3	0.2	0	99.8	0	99.8
	4	0	0	100	0	100
	6	0	0	100	0	100

[a] Yields of summed S_N2 Products $\%(A + B)$ and the yield of the E2 $\%D$ are normalized. [b] Norm $\%(A + B) = 100\times$(Meas $\%A$ + Meas $\%B$)/(Meas $\%A$ + Meas $\%B$ + Meas $\%D$). [c] Norm $\%D = 100\times$(Meas $\%D$)/(Meas $\%A$ + Meas $\%B$ + Meas $\%D$).

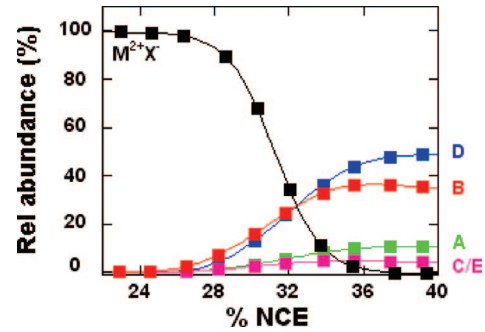

Figure 2. Plot of relative ionic species abundances (rel abundance (%)) against the percent normalized collision energy (%NCE) for breakdown curve (150 data points, only 15 shown for clarity) of 16-6-16 CF_3CO_2 ($M^{2+}X^-$) fitted with a Boltzmann sigmoidal function. Curves for S_N2 (A and B) and E2 (D) products were fitted to aid the eye (140 points, 15 shown). Product yields were obtained graphically at $\%CE_0$ from the plateau. Note: the curve labeled C/E could be attributed to either S_N2 (C) or E2 (E) products (see text).

Results

ESI-MS spectra of 16-*n*-16 2X surfactants in the positive mode (ESI+) give signals for both the gemini dication M^{2+} and the gemini pair $M^{2+}X^-$. Figure 1A shows a typical spectrum obtained for the 16-6-16$^{2+}CF_3CO_2^-$ pair from a methanolic solution of the 16-6-16$^{2+}2CF_3CO_2^-$ salt. In the tandem MS experiments, $M^{2+}X^-$ ions were isolated in the ion trap by their m/z ratio.

TABLE 2: BSSE Corrected Enthalpies (ΔH, kcal mol^{-1}) and Free Energies (ΔG, kcal mol^{-1}) of Ion Pair formation for $M^{2+}X^{-}$[a]

	F^-		Cl^-		Br^-		I^-	
anion→ cation↓	ΔH	ΔG	ΔH	ΔG	ΔH	ΔG	ΔH	ΔG
2	−195.6	−185.9	−167.5	−158.0	−159.7	−150.8	−151.7	−142.6
3	−187.6	−177.7	−160.5	−151.8	−153.1	−144.6	−146.1	−137.8
4	−181.5	−170.0	−152.9	−143.7	−156.4	−147.0	−138.0	−129.1

[a] Corrected for zero point energy and thermal effects at 298.15 K.

Schemes 2 and 3 show the multiple reaction pathways for formation of products from fragmentation of a single $M^{2+}X^-$ pair by competing S_N2 and E2 reactions, respectively, that appear in Figure 1C,D. The intensities of the A, B, and D peaks at CE_0 in Figure 1D were averaged with peak intensities for these products from two additional MS experiments to calculate the product yields in Table 1 below. Unlabeled peaks are from impurities from the solvent and appear in many of the mass spectra for the salts. The color scheme for the reaction pathways and products identifiable by MS is used throughout the text to aid in identifying products from the various fragmentation pathways.

Reactions with the methylenes on the hexadecyl chain generally gave only small yields, for example, peak C, in Figure 1D; therefore, our primary focus is on S_N2 and E2 reactions with the methylenes adjacent to the two quaternary ammonium nitrogens and the nitrogen methyls. The structure of and notation for the gemini surfactants and bolaform salts in all Schemes are based on using subscript "*n*" to indicate the number of methylenes in the spacer between the two quaternary ammonium nitrogens. No signals were observed for M^{2+} in the ERMS experiments indicating that the $M^{2+}X^-$ pairs only fragment and do not dissociate via $M^{2+}X^- \rightarrow M^{2+} + X^-$. This is not surprising given that the calculated $\Delta H^{\ddagger}$ values for ion-pair fragmentation are on the order of +10 to +30 kcal mol^{-1}, whereas the calculated enthalpies for the breakup of ion pairs, the reverse of ion-pair formation (see Table 2), range from about +140 to +200 kcal mol^{-1}.

In the ERMS experiments, the kinetic energy of $M^{2+}X^-$ was increased in the trap by resonant excitation of the ion pair using helium as the buffer gas with gradually increasing collision energy at constant temperature and the peak intensities of the $M^{2+}X^-$ pair and product ions are obtained for each step of energy. Typical MS/MS spectra are shown in Figure 1, spectra B, C, and D, for three different collision energies: CE_{100} (100% of the precursor ion, $M^{2+}X^-$), CE_{50} (50%), and CE_0 (0%), respectively.

Relative abundances versus %NCE were obtained for each spacer length and anion of the 16-*n*-16$^{2+}X^-$ pair, Scheme 1, from CE_{100} to CE_0. Figure 2 illustrates the results for the 16-6-16$^{2+}CF_3CO_2^-$ pair. Product ratios are obtained from the relative abundances in each spectrum compared to that at CE_0 and the effect of spacer length and anion type on the yields of S_N2 and E2 products are presented below. The relative abundances at each spacer length and anion type for all 22 ERMS experiments are compiled as normalized percent yields in the Supporting Information, Table S2.

Fragmentation Energy of the Precursor Ion $M^{2+}X^-$. Figure 3 compares %NCE values of the precursor ions at CE_{50} for increasing spacer length and for different X^-. F^- has the lowest and PF_6^- the highest CE_{50}, consistent with their gas-phase enthalpies of ionization, $\Delta H_{acid}°$, of their conjugate acids (see Supporting Information, Table S4). The CE_{50} values for Cl^-, Br^-, I^-, $CF_3CO_2^-$, and NO_3^- are similar, and they form two plateaux, each with a significant jump in value between spacer lengths $n = 3$ and 4. For some of these ions, this increase is consistent with the large shifts in product yields from the E2 to S_N2 pathway (see below). The results for F^- are complex. The $M^{2+}F^-$ pairs at $n = 4$ and 6 fragment at very low CE_{50} and even $M^{2+}F^-$ pairs for $n = 2$ and 3 could not be isolated. Only signals for E2 products (D) were observed in ESI-MS experiment, probably because they decomposed in solution ($n = 2$) or between the spray and ion trap ($n = 3$).

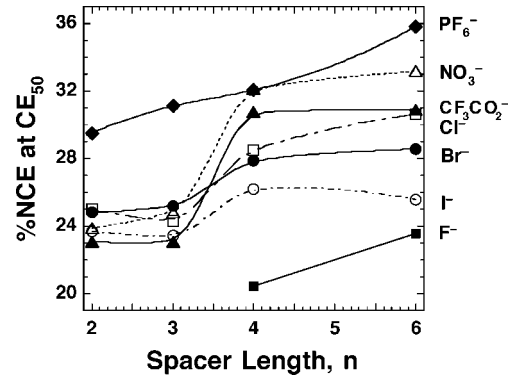

Figure 3. Normalized collision energy at CE_{50} as a function of spacer length and counterion type. Lines are drawn to aid the eye.

Competing E2 and S_N2 Reactions. Table 1 lists the measured yields for S_N2 products, A and B, the E2 product, D, and the normalized percent yield of the sum of products A + B and of D (see Table 1 footnotes for method of calculation). The total yields from these three pathways are assumed to be 100% for all dication spacer lengths and anions. We did not include products from pathways c + e in the interpretation of the results because the total yields are small and we could not distinguish between products from the S_N2 (pathway c, Scheme 2) and E2 (pathway e, Scheme 3) reactions occurring on the hexadecyl chains of the gemini surfactants. The cationic products from these two reactions are identical and the uncharged products cannot be identified by MS. The total yields of products from pathways c and e are usually small (average 3.2% for all 22 ERMS experiments).

Figure 4A,B summarizes the normalized percent yields from the sum of substitution products from pathways a and b (S_N2), and elimination products from pathway d (E2) (last two columns in Table 1). I^- only gives products from S_N2 reactions at all spacer lengths. The Cl^-, Br^-, NO_3^-, and $CF_3CO_2^-$ anions give both S_N2 and E2 products depending on spacer length, and overall the yields of E2 products decrease while S_N2 products increase with increasing spacer length for these ions. PF_6^- and F^- give only E2 products. Table 1 also shows that yields from the competing S_N2 reaction at methyl (S_N2 product B) are generally small, except for $n = 6$.

Taken together, several trends are apparent in product yields (Table 1 and Figure 4A,B) and in the CE_{50} values (Figure 3) for all the anions except F^- and PF_6^-: (a) as the spacer length increases from 2 to 6, the dominant reaction switches from E2 to S_N2; (b) the CE_{50} values jump between spacer lengths 3 and 4; (c) the Cl^-, $CF_3CO_2^-$, and NO_3^- anions show the biggest

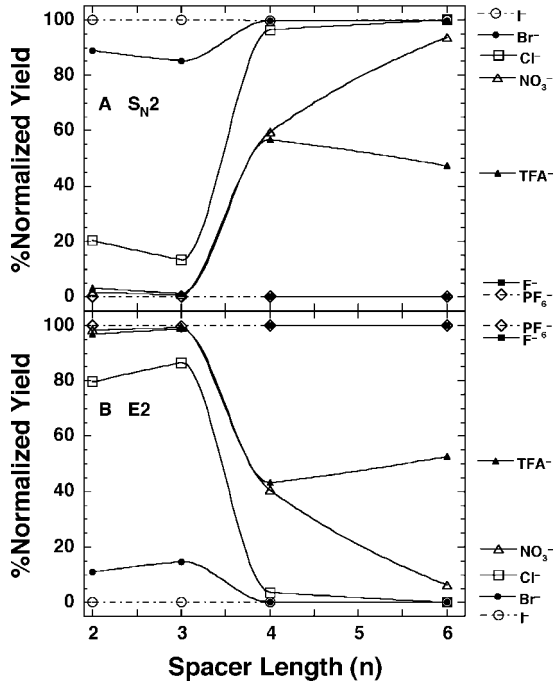

Figure 4. Normalized percent yields versus spacer length, *n*, for each counterion: (A) S_N2 products (A + B), and (B) E2 product D. Data taken from Table 1, columns 6 and 7. Lines are drawn to aid the eye.

shift from E2 to S_N2 products between $n = 3$ and 4, while I^- and Br^- form S_N2 products almost exclusively; and (d) in general the yields from substitution on methyl for $n = 2-4$ are small, but when $n = 6$, attack on methyl tends to become the dominant product. F^- is the strongest base and has the lowest CE_{50} and gives only E2 products, consistent with the trends shown by the other anions. PF_6^- is the weakest base, which is consistent with it having the highest CE_{50}, but it only gives E2 products. We suspect that the PF_6^- reacts by a different mechanism (see Supporting Information).

DFT Calculations: The Halide Ions. Scheme 4 summarizes relative energy changes that were obtained by DFT calculations in the gas-phase for the formation of the ground-state $M^{2+}X^-$ structures of the 1-*n*-1 2X bolaform ion pairs and for the competing reactions leading to the transition structures for the S_N2 (pathway a) and the syn- and anti-E2 (pathway d) reactions. DFT calculations were also carried out for the same reactions for the M^+X^- pairs (M = ethyltrimethylammonium, $X^- = F^-$, Cl^-, Br^- and I^-) to probe the effect of the second quaternary ammonium cation on the activation enthalpies of the $M^{2+}X^-$ pairs. The overall energy changes and mechanisms for the related reactions of M^+X^-, that is, syn-E2, anti-E2 eliminations, and S_N2 substitutions are analogous to those for $M^{2+}X^-$, Scheme 4. Tables 2−4 summarize the DFT calculation results. Table 2 lists enthalpies (ΔH) and free energies (ΔG) for formation of ion pairs. As the spacer length becomes longer and as the halide ion becomes larger and less basic, the complexes tend to become less stable, that is, ΔH and ΔG become less negative. However, ΔH values for the formation of the $M^{2+}Cl^-$ and $M^{2+}Br^-$ pairs are similar and differ by only about 5−8 kcal mol^{-1}; with spacer lengths 2 and 3, $M^{2+}Cl^-$ is more stable with the more negative ΔH and ΔG, and at spacer length 4, $M^{2+}Br^-$ is more stable. Note that the ΔG values of these ground-state structures are generally about 8−10 kcal mol^{-1} less negative than the ΔH values.

The DFT calculated enthalpies of activation, $\Delta H^‡$, values for S_N2 and E2 (syn and anti) pathways for $M^{2+}X^-$ are listed in Table 3, and ΔH and $\Delta H^‡$ values for the M^+X^- pairs are in Table 4. Figure 5 is a graphical summary of the $\Delta H^‡$ results for easier visualization of the trends. The $\Delta H^‡$ values for the syn- and anti-E2 reactions are numerically similar, although typically the anti $\Delta H^‡$ values are lower, except for 1-2-$1^{2+}F^-$, differing in energy from the syn values by about 0−3 kcal mol^{-1}. When the anti-E2 $\Delta H^‡$ values (except for the 1-2-$1^{2+}F^-$ pair) are compared with the $\Delta H^‡$ values for S_N2 reactions, several trends are evident. The $\Delta H^‡$ values for S_N2 reactions are virtually independent of spacer length and anion type (see Figure 5). The average value is 20.4 kcal mol^{-1} (12 $\Delta H^‡$ values) and the standard deviation is 0.65 kcal mol^{-1}. The $\Delta H^‡$ values for the E2 eliminations, to the contrary, increase significantly with decreasing anion basicity (see Supporting Information) from a minimum of 12.1 kcal mol^{-1} for 1-2-$1^{2+}F^-$ (syn-E2 $\Delta H^‡$ value) to a maximum of 31.8 kcal mol^{-1} for 1-4-$1^{2+}I^-$, an increase of 19.7 kcal mol^{-1}. The E2 $\Delta H^‡$ values for Cl^-, Br^-, and I^- are greater than those for S_N2, Figure 5. $\Delta H^‡$ values for E2 reactions also depend on spacer length. As *n* increases from 2 to 4, $\Delta H^‡$ increases about 3−5 kcal mol^{-1} for Cl^-, Br^- and I^-, and about 10 kcal mol^{-1} for F^-. $\Delta H^‡$ for the E2 reaction of F^- is less than that of its S_N2 reaction by up to 10 kcal mol^{-1} at $n = 2$, 3, but at $n = 4$, $\Delta H^‡$ is about the same for both S_N2 and E2. The $\Delta H^‡$ for the M^+X^- pairs fall in the middle of the curves for the $M^{2+}X^-$.

The ΔH and $\Delta H^‡$ for M^+X^- pairs summarized in Table 4 were obtained to evaluate the effect of the second charge on the calculated ΔH and $\Delta H^‡$ values of the bolaforms. The ΔH values for each X^- are about 55−60% smaller than that for the same X^- for the gemini listed in Table 3 at all three spacer lengths, that is, adding a second positive charge makes the ground-state ion-pair structure almost twice as stable. The $\Delta H^‡$ values for S_N2 reactions of M^+X^- pairs are similar in value to those for $M^{2+}X^-$ pairs but decrease slightly (ca. 2 kcal mol^{-1}) with increasing X^- size (see open triangles in Figure 5). The average enthalpies for the M^+X^- pairs are $\Delta H^‡ = 21.1 \pm 1.0$ (4 values) which are in good agreement with the average value of $\Delta H^‡ = 20.4 \pm 0.65$ for the $M^{2+}X^-$ pairs noted above. The $\Delta H^‡$ values for E2 reactions of M^+X^- pairs increase with the decreasing basicity of X^- and are numerically similar to those for the E2 reactions of the $M^{2+}X^-$ pairs in Table 3 (see solid diamonds in Figure 5). Note that $\Delta H^‡$ values for the E2 reaction of F^-, whose basicity is significantly greater, are significantly lower than the relatively similar $\Delta H^‡$ values and basicities for Cl^-, Br^-, and I^- in the E2 reaction. The same pattern is observed in their gas phase ionization energies (Supporting Information, Table S4). Finally, the $\Delta H^‡$ values for syn elimination of M^+F^- pairs, for example, 1-2-$1^{2+}F^-$, are significantly lower than that for anti, while for the other three halide ions they are essentially the same as they are for the $M^{2+}X^-$ pairs in Table 3. These calculations show that second charge on the dication has little effect on activation energies and that the ground structure and transition structure interactions are governed primarily by electrostatics and anion basicity (see Discussion). Note that $\Delta H^‡$ value for the S_N2 reaction at the methyl group by I^- is only about 2 kcal mol^{-1} less the reaction at methylene. We assume that the differences for the other halide ions will be similar.

Discussion

Scheme 5 is a compact visual summary of the two basic structure−reactivity trends for the competing S_N2 and E2

SCHEME 4: Competing S_N2 and E2 Pathways Showing the Transitions from the Free Ions to the Ground Structure Ion-pair, $M^{2+}X^-$, to the syn- and anti-E2 and S_N2 Transition Structures[a]

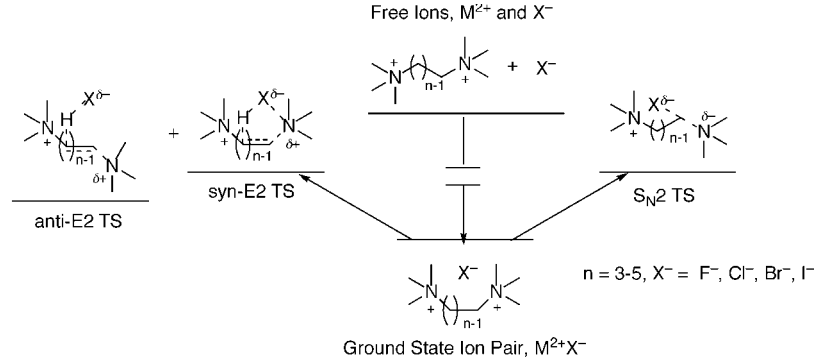

[a] Notation for the number of spacer methylenes is as in Schemes 2 and 3.

TABLE 3: Activation Enthalpies ($\Delta H^{\ddagger}$, kcal mol^{-1}) for E2 and S_N2 Reactions of $M^{2+}X^-$. Corrected for Zero Point Energy and Thermal Effects at 298.15 K

	2			3			4		
spacer length	E2		S_N2	E2		S_N2	E2		S_N2
halide/RX	syn	anti		syn	anti		syn	anti	
F^-	12.1	15.4	18.7	15.3	11.4	20.6	23.0	21.2	20.4
Cl^-	24.2	24.1	21.1	25.1	23.7	21.1	30.4	28.0	20.4
Br^-	28.9	28.4	20.4	32.3	30.4	20.8	33.7	31.8	20.6
I^-	28.2	27.3	19.8	35.6	30.4	20.6	33.6	31.8	20.2

TABLE 4: Enthalpies of Ion Pair Formation (ΔH, kcal mol^{-1}) for Halide Pairs, M^+X^-, and Activation Enthalpies ($\Delta H^{\ddagger}$, kcal mol^{-1}) for the Reactions of X^- with Ethyltrimethylammonium Halides, M^+X^-: S_N2 (on $CH_3\underline{CH_2}N(Me)_3^+$ and syn- and anti-E2 Eliminations (on $\underline{CH_3}CH_2N(Me)_3^+$). Corrected for Zero Point Energy and Thermal Effects at 298.15 K

anion→ cation↓	F^- ΔH	Cl^- ΔH	Br^- ΔH	I^- ΔH
M^+X^-	−111.4	−90.5	−87.0	−81.0
M^+X^-	$\Delta H^{\ddagger}$	$\Delta H^{\ddagger}$	$\Delta H^{\ddagger}$	$\Delta H^{\ddagger}$
E2 syn	15.6	26.5	29.3	29.9
E2 anti	21.0	27.3	29.3	29.1
S_N2	22.6	21.5	20.3	19.9 (17.4[a])

[a] Reaction at $CH_3CH_2N(\underline{CH_3})_3^+$.

reactions with anion type and spacer length found from the MS experiments with the gemini surfactants, 16-*n*-16 2X, $n = 2-6$, $X^- = F^-$, Cl^-, Br^-, I^-, $CF_3CO_2^-$, NO_3^-, and PF_6^-, and from DFT calculations for the bolaform salts, 1-*n*-1 2X, $n = 2-4$, $X^- = F^-$, Cl^-, Br^-, and I^-: (a) increasing the number of methylenes in the spacer shifts the reaction from E2 (syn or anti) to S_N2 (reaction on methyl or methylene) products; and (b) increasing anion basicity shifts the reaction toward the elimination pathways (anti or syn). These trends do not correlate with the calculated enthalpies and free energies of $M^{2+}X^-$ pair formation. For the halide ions listed in Table 2, ΔH and ΔG decrease steadily from 1-2-1^{2+}F$^-$ to 1-4-1^{2+}I$^-$ by about 60 kcal mol^{-1} with increasing spacer length and decreasing anion basicity. A similar anion basicity dependence is observed for the monocations in Table 4. The estimated values of $T\Delta S$ for formation of an $M^{2+}X^-$ pair structure, Table 2, range from −8 to −10 kcal mol^{-1}, which is a significant change in $T\Delta S$, but only about 5−8% of the change in ΔH. Consequently, for individual ion pairs, entropy loss makes only a small contribution to ΔG of pair formation and does not affect the calculated trends in ΔH (and ΔG).

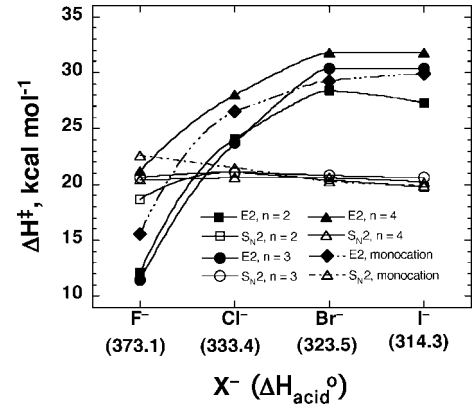

Figure 5. $\Delta H^{\ddagger}$ values versus halide ion type for the S_N2 and E2 reactions of the bolaform, $M^{2+}X^-$ (solid lines), and ethyltrimethylammonium halide, M^+X^-, pairs (dashed lines) for spacer lengths $n = 2-4$; see legend. Data are in Tables 3 and 4. Lines are drawn to aid the eye. $\Delta H_{acid}°$ is the gas phase enthalpy of ionization of the halo acids (see Supporting Information).

SCHEME 5: Dependence of E2 and S_N2 Pathways on Counterion Type, X^-, and Spacer Length: Gemini (R = $C_{16}H_{33}$, $n = 2-6$), Bolaform (R = CH_3, $n = 2-4$)

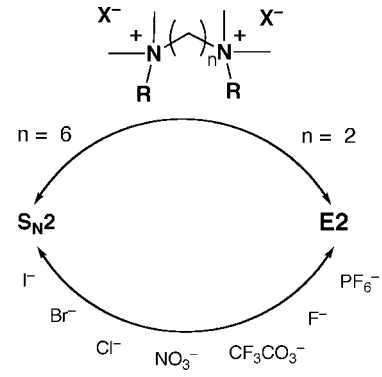

The DFT calculated $\Delta H^{\ddagger}$ values listed in Table 3 for the $M^{2+}X^-$ pairs, in Table 4 for the M^+X^- pairs, and shown graphically in Figure 5 provide insight into the dependence of the transition from E2 to S_N2 products listed in Table 1 on structures of the ion pairs. (a) $\Delta H^{\ddagger}$ values for the E2 reaction increase significantly with decreasing X^- basicity and increase modestly with spacer length. (b) The $\Delta H^{\ddagger}$ values for the S_N2 reaction, to the contrary, are virtually independent of anion basicity. This result stands in stark contrast to nucleophile

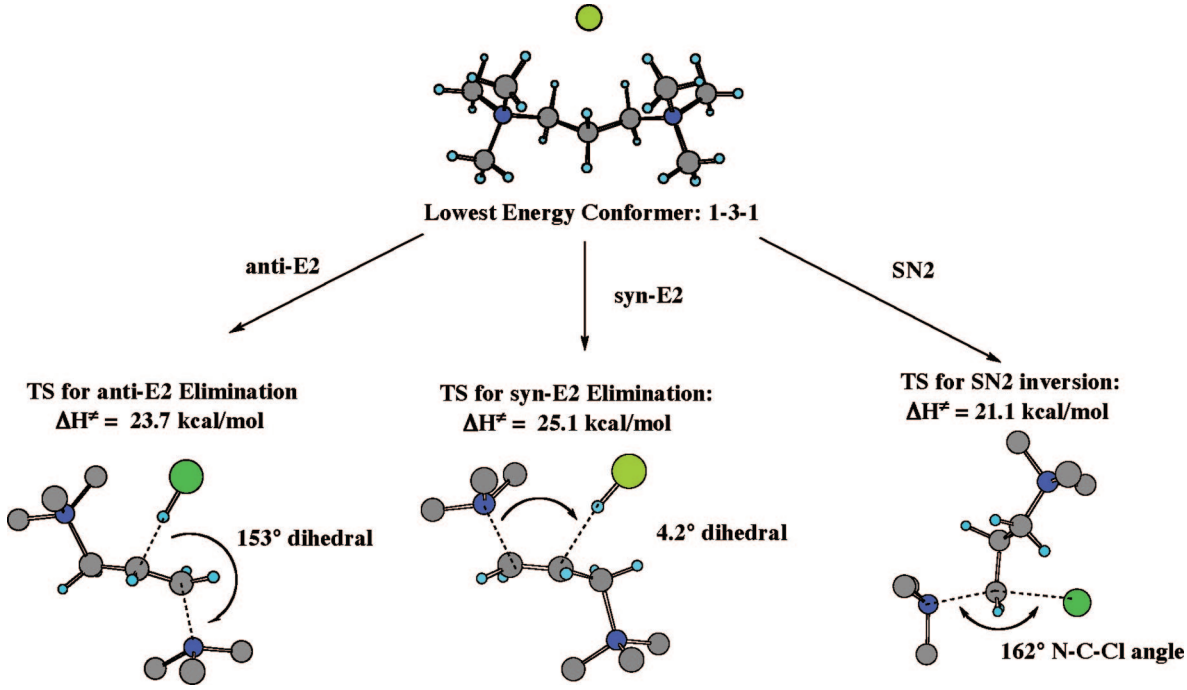

Figure 6. Ground state and transition structures for S_N2 and E2 reactions of the 1-3-$1^{2+}Cl^-$ pair. Protons on some N-methyl groups in the transition structures have been deleted for clarity.

reactivity orders in solution that are strongly dependent on solvent polarity. For example, acetone, which induces ion pairing of anionic nucleophiles with neutral organic substrates, reverses the nucleophilicity order found in polar, protic solvents: $I^- > Br^- > Cl^-$.[38,58,59] Gronert and Fong found similar $\Delta H^‡$ values for the S_N2 reaction of isobutyltrimethylammonium with acetate ion in the gas phase at the HF/6-31+G* and MP2/6-31+G(d) levels.[60] The $\Delta H^‡$ values for E2 reaction of these ions are larger than those for S_N2, as they are for reactions of methoxide ion with β-halo substituted ethyl bromides.[61] (c) The calculated $\Delta H^‡$ values for the S_N2 and E2 reactions are qualitatively consistent with the observed E2 and S_N2 product yields for the halide ions in Table 1; F^- gives primarily E2 products and Br^- and I^- give predominately or completely S_N2 products (Table 1). (d) Finally, while the second cation strongly stabilizes the $M^{2+}X^-$ pairs compared to the M^+X^- pairs (Tables 2 and 4) the presence of the second cation has almost no effect on $\Delta H^‡$ for reaction of the $M^{2+}X^-$ and M^+X^- pairs (see Tables 3 and 4 and Figure 5). Gronert demonstrated for two different sets of reactants that when the second charge of a twin-charge nucleophile is about 15 Å from the first, the transition structure energies are similar to that of the monovalent nucleophile analog.[27,28] However, we found that S_N2 reactions of $M^{2+}X^-$ pairs show no dependence on the presence of a second charge or on the distance between the two cations or nucleophile type.

The switch from dominant E2 to the S_N2 pathways on going from F^- to Cl^-, Br^-, and I^- is also consistent with several sets of published results that show that first row anions promote elimination and second row anions promote substitution in gas-phase reactions. For example, F^- tends to promote E2 eliminations with ethyl chloride and PH_2^-, which has the same gas-phase basicity, and has a lower S_N2 than E2 transition barrier.[62] Similarly, alkoxide and alkylthiolate nucleophiles of the same gas-phase basicities promote E2 and S_N2, respectively.[31] Thus the transition from S_N2 to E2 for the halide ions might also be associated with the increasing size and/or polarizability of the electron cloud around the nucleophile, consistent with the conclusion of Bickelhaupt et al. that for a given electrophile, the electronic structure of the base determines the S_N2/E2 selectivity.[63]

DFT calculations fail to agree with MS product yields in only a few cases. The DFT calculations predict only S_N2 products for Cl^-, but MS experiments show that only E2 products are formed for spacer lengths 2 and 3 (Table 1). Also, the calculated $\Delta H^‡$ value for 1-4-$1^{2+}F^-$predicts about 50:50 S_N2/E2 (Figure 5) whereas experimentally only elimination is observed. These differences in the MS and DFT results probably reflect the fact that competitive product yields depend on $\Delta G^‡$ for the entire ensemble of ion pairs reacting in the gas-phase and that individual DFT calculations do not allow for estimates of $\Delta S^‡$ and $\Delta H^‡$ for the ensemble of reacting $M^{2+}X^-$ pairs (see below).

E2 and S_N2 Ground and Transition Structures. Figure 6 shows the calculated ground and competitively formed transition structures for the S_N2 and E2 (syn and anti) pathways for 1-3-$1^{2+}Cl^-$ and are representative of all the 1-*n*-$1^{2+}X^-$ pairs (n = 2−4, X^- = F^-, Cl^-, Br^-, I^-) and their reactions summarized in Scheme 4. Considerable intramolecular motion is required to overcome the strong binding energies of the ion pairs (Table 2) between the Cl^- and the trimethylamine groups to attain the calculated transition structure geometries for elimination and substitution. In the ground structure, the anion is nested in an environment composed of hydrocarbon-like methyls and methylenes, and it is flanked by two positive charges dispersed over the methyl and α-methylene groups. The transition structures are considerably more open with one of the ammonium groups rotated away from the anion.

E2 Reactions, Dependence of Ground and Transition Structures on Anion Basicity and Spacer Length. The E2 reaction requires near simultaneous cleavage of the C−N and C−H bonds and the formation of H−X and C=C bonds. Table 5 (A and B) lists selected calculated geometric parameters for the syn- and anti-E2 transition structures with increasing spacer length and varying halide ion type. The changes in C···N, C···H, and H···X transition structure

TABLE 5: Selected Geometric Parameters for Gas-Phase Reactions of $M^{2+}X^-$: (A) anti-E2; (B) syn-E2; and (C) S_N2

	$n = 2$				$n = 3$				$n = 4$			
(A) X^-	C···N	C···H	H···X	NCCH	C···N	C···H	H···X	NCCH	C···N	C···H	H···X	NCCH
F^-	1.611	1.400	1.329	170.7°	1.627	1.425	1.127	157.5°	1.858	1.469	1.109	176.5°
Cl^-	1.853	1.586	1.458	167.2°	1.842	1.739	1.403	153.3°	2.131	1.491	1.531	176.2°
Br^-	2.086	1.555	1.653	162.9°	2.077	1.706	1.608	156.1°	2.388	1.529	1.689	176.1°
I^-	2.076	1.551	1.847	161.8°	2.000	1.747	1.785	152.5°	2.404	1.528	1.876	174.2°
	$n = 2$				$n = 3$				$n = 4$			
(B) X^-	C···N	C···H	H···X	NCCH	C···N	C···H	H···X	NCCH	C···N	C···H	H···X	NCCH
F^-	2.006	1.731	0.992	2.83°	1.980	1.670	1.011	11.0°	2.026	1.523	1.070	7.11°
Cl^-	2.011	1.742	1.395	6.88°	1.800	2.034	1.334	4.17°	2.324	1.436	1.551	3.95°
Br^-	2.323	1.542	1.653	8.79°	2.089	1.648	1.617	5.70°	2.602	1.428	1.737	3.15°
I^-	2.355	1.506	1.865	8.67°	2.470	1.469	1.911	18.2°	2.639	1.422	1.926	4.35°
	$n = 2$				$n = 3$				$n = 4$			
(C) X^-	X···C	C···NR_3	X···C···NR		X···C	C···NR_3	X···C···NR		X···C	C···NR_3	X···C···NR	
F^-	1.992	1.878	163.5°		1.972	1.949	165.2°		1.959	1.995	165.0°	
Cl^-	2.460	2.006	158.1°		2.428	2.065	161.7°		2.428	2.122	157.5°	
Br^-	2.652	2.024	155.8°		2.609	2.089	160.6°		2.584	2.151	159.6°	
I^-	2.894	2.023	153.1°		2.838	2.091	159.0°		2.824	2.149	155.8°	

TABLE 6: Distances (Å) between the Nucleophiles, X^-, and the Leaving Group, N ($-N(Me)_3$), in the Ground and Transition Structures of the S_N2 Reactions and Their Difference, Δ[a]

	$n = 2$			$n = 3$			$n = 4$		
A	G[b]	T[b]		G[b]	T[b]		G[b]	T[b]	
X^-	X···N	X···N	Δ	X···N	X···N	Δ	X···N	X···N	Δ
F^-	3.28	3.83	0.55	3.27	3.89	0.62	3.26	3.92	0.66
Cl^-	3.90	4.39	0.49	3.88	4.44	0.56	3.89	4.47	0.58
Br^-	4.11	4.57	0.46	4.07	4.63	0.56	4.05	4.66	0.61
I^-	4.36	4.79	0.43	4.29	4.85	0.56	4.26	4.86	0.40
	average $\Delta = 0.48 \pm 8\%$			average $\Delta = 0.58 \pm 5\%$			average $\Delta = 0.59 \pm 12\%$		

B	G[b]	T[b]	
X^-	X···N	X···N	Δ
F^-	2.97	3.90	0.93
Cl^-	3.61	4.42	0.81
Br^-	3.84	4.59	0.75
I^-	4.09	4.82	0.73
		average $\Delta = 0.81 \pm 9\%$	
C	4.06	4.74	0.68

[a] (A) S_N2 reactions of $M^{2+}X^-$; (B) S_N2 reactions of M^+X^- on methylene; and (C) S_N2 reactions of M^+X^- on methyl. [b] G = ground structure, and T = transition structure.

bond lengths on going from F^- to I^- are generally significant, and with some exceptions both C···N and H···X bond lengths increase. However, the C···H bond lengths and dihedral bond angles (NCCH) are variable with no simple correlations with X^- type, both for anti-E2 (Table 5A) and syn-E2 (Table 5B) pathways. The changes in bond lengths and dihedral angles with increasing spacer length in the transition structures are modest for both syn- and anti-E2 reactions. On the other hand, the dependence of H···X bond lengths on X^- basicity and spacer length are highly consistent with $\Delta H^‡$ changes within a given spacer length series, that is, stronger bases lead to shorter C···H distances and lower $\Delta H^‡$ values. The possibility of elimination proceeding via an E1cb (elimination, unimolecular, conjugate base) mechanism[38] was ruled out for the most likely candidate,1-2-$1^{2+}F^-$, on the basis of intrinsic reaction coordinate computations leaving syn-E2 elimination as the most likely pathway (Table 3). These results showed that C−H bond cleavage is accompanied by simultaneous lengthening of the C−N bond (Table 5) and C=C bond formation.[64]

S_N2 Reactions, Dependence of Ground and Transition Structures on Anion Basicity and Spacer Length. Table 5C summarizes the transition structures in the S_N2 reactions, Figure 6. The changes in the X···C···NR bond angles and C···NR_3 bond lengths are both modest with increasing spacer length and halide ion type. The X···C bond lengths are also virtually independent of spacer length, but increase by almost one Å on going down the table from F^- to I^-.

Table 6 summarizes the DFT calculated nucleophile, X^- (X)—leaving group, $N(CH_3)_3$ (N) distances, (X···N), distances for the bolaform ion pairs, $M^{2+}X^-$, for the ground and transition structures. Note that the X···N as well as the X···C distances increase about 1 Å with anion size on going from F^- to I^- and vary only slightly with spacer length. The difference, Δ, between the ground, G, and transition, T, structures X···N atom distances reflects the change in the strength of the electrostatic interaction between the anionic nucleophile and cationic headgroup. Δ decreases slightly with X^- size, but is approximately constant (average value of 0.55 ± 8% for all X^- and spacer lengths), consistent with the

almost constant calculated values of $\Delta H^{\ddagger}$. The same trend is observed for the monovalent cation, M^+X^-, Table 6B, except that the values of Δ are a little larger. Taken together, these results suggest that in these S_N2 reactions, the increase in X^- size and change in polarization must have similar effects on ground and transition structure energies such that $\Delta H^{\ddagger}$ remains approximately constant.

Entropic Contributions in Competing S_N2 and E2 Reactions and in Competing S_N2 Reactions at Methylene and Methyl. A complete quantitative interpretation of factors controlling the $\Delta G^{\ddagger}$ values for the structure−reactivity relationships for the competitive gas-phase fragmentations requires both $T\Delta S^{\ddagger}$ and $\Delta H^{\ddagger}$ values for the ensemble of reacting $M^{2+}X^-$ pairs. Obtaining these thermodynamic values is beyond the scope of this work, although consideration of entropic factors for the ensemble of reacting $M^{2+}X^-$ pairs may provide a reasonable bridge between the differences in MS product distributions and the single structure complex calculations by DFT and also a reasonable explanation for the increase in substitution at methyl as the spacer length increases (see Supporting Information).

Conclusions

Dicationic−monoanion pairs, $M^{2+}X^-$, formed from hexadecyldiyl-α,ω-bis(dimethylalkylammonium) dianion surfactants ("gemini", 16-*n*-16$^{2+}X^-$) provide unique systems for studying competitive S_N2 and E2 reactions in the gas-phase. Our combined MS and DFT results provide new insight into the factors controlling competitive S_N2 and E2 reactions. All the $M^{2+}X^-$ pairs investigated, except some F^- pairs, are stable in the ion trap of spectrometer, consistent with DFT computations of the bolaform analogs that show that $M^{2+}X^-$ pairs are extremely stable in the gas phase. Products from collision induced intramolecular fragmentations in the mass spectrometer show that S_N2 substitution at the α-methylene and nitrogen methyl competes with E2 elimination at the β-C−H bond. Several trends are observed. As the anions ($X^- = F^-$, Cl^-, $CF_3CO_2^-$, NO_3^-, Br^-, I^-, and PF_6^-) become less basic and as the spacer length increases ($n = 2$, 3, 4, and 6), the major product shifts from E2 toward S_N2 with the exceptions of PF_6^- and F^-, which always gives elimination. As the spacer length increases, the major product from S_N2 reaction shifts from reaction at α-methylene in the spacer to methyl on the ammonium nitrogen.

DFT calculated enthalpies of activation, $\Delta H^{\ddagger}$, for reaction of dication-monoanion, $M^{2+}X^-$, pairs and enthalpies of pair formation, ΔH, for the bolaform salts, bis(trimethyl)-α,ω-alkanediammonium halide pairs ($X^- = F^-$, Cl^-, Br^-, I^-) and spacer lengths ($n = 2$, 3, and 4) provide a qualitative rationale for the MS results with the gemini surfactants. $\Delta H^{\ddagger}$ values for the S_N2 reaction are virtually independent of X^- type and spacer length, but $\Delta H^{\ddagger}$ values for the E2 reaction increase significantly with decreasing X^- basicity and increase modestly with spacer length, which is consistent with an increase in β-C−H bond strength in the elimination reaction because the stabilizing positive charge of the second ammonium group moves further from breaking C−H bond. Additional DFT calculations on model monocation salts, ethyltrimethylammonium halides, show that the trends in $\Delta H^{\ddagger}$ values of S_N2 and E2 reactions are only modestly affected by the presence of the second charge on the bolaform ion pairs.

The trend in ΔH for $M^{2+}X^-$ pair formation (most stable when $X^- = F^-$ to least stable when $X^- = I^-$) is the reverse of that normally observed for specific ion effects on the properties of cationic surfactants in aqueous solution. Future studies of microhydration effects on the specific counterion effects on the gas-phase properties of gemini surfactants should provide new insight into the importance of headgroup hydration on the specific ion interactions controlling the stabilities of surfactant micelles. Measurement of the temperature dependence of the rate constants for fragmentation of these ion pairs should provide important information on the activation free energies, enthalpies, and entropies of these reactions.

Acknowledgment. To Janos Fendler and his zest for life, science, and good company. The work in Bordeaux was supported by the Centre National de la Recherche Scientifique (CNRS), the University of Bordeaux I, and the Conseil Régional d'Aquitaine. R.O., C.A. and B.P. thank Katell Bathany for her help in MS measurements. The work at Rutgers was supported by the National Center for Supercomputer Applications for allocation time (Grant TG-CHE080003N) and the Organic Chemical Dynamics division of the National Science Foundation for financial support (CHE-0411990). Portions of the manuscript are subjects of Ph.D. theses by C. Aimé and B. Plet, University Bordeaux I. L.S.R. and R.R.S. thank Tom Chapin for crucial software assistance and Clifford Bunton and Karsten Krogh-Jespersen for extremely helpful discussions.

Supporting Information Available: CID-MS results for all 16-*n*-16 2X ion pairs; details on yields of all MS products and normalized product yields; ^1H and ^{13}C spectra of gemini surfactants; gas phase ionization energies and solution acidity constants of conjugate acids of X^-; E2 and S_N2 activation enthalpies at B3LYP and MP2 levels; computed enthalpies (Hartrees) for all ground and transition structures corrected for zero point and thermal effects; calculated activation energies for the E2 and S_N2 reactions of the bolaform salts; proposed E2 mechanism for PF_6^-; and entropic contributions for S_N2 and E2 reactions and S_N2 reactions at methylene and methyl are provided. This material is available free of charge via the Internet at http://pubs.acs.org.

References and Notes

(1) Gronert, S. *Mass Spectrom. Rev.* **2005**, *24*, 100.
(2) Romsted, L. S. *Langmuir* **2007**, *23*, 414.
(3) Kunz, W.; Lo Nostro, P.; Ninham, B. W. *Curr. Opin. Colloid Interface Sci.* **2004**, *9*, 1.
(4) Tobias, D. J.; Hemminger, J. C. *Science* **2008**, *319*, 1197.
(5) Hofmeister, F. *Naunyn-Schmiedeberg's Arch. Exp. Pathol. Parmakol.* **1888**, *24*, 247.
(6) Collins, K. D.; Washabaugh, M. W. *Q. Rev. Biophys.* **1985**, *18*, 323.
(7) Collins, K. D.; Neilson, G. W.; Enderby, J. E. *Biophys. Chem.* **2007**, *128*, 95.
(8) Anderson, C. F.; Record, M. T. J. *Annu. Rev. Biophys. Biophys. Chem.* **1990**, *19*, 423.
(9) Eisenman, G. *The Glass Electrode*; Interscience Reprint, Interscience: New York, 1965.
(10) Diamond, J. M.; Wright, E. M. *Annu. Rev. Physiol.* **1969**, *31*, 581.
(11) Rosen, M. J. *Surfactants and Interfacial Phenomena*, 3rd ed.; John Wiley & Sons: New York, 2004.
(12) Lindman, B. Physico-Chemical Properties of Surfactants. *In Handbook of Applied Surface and Colloid Chemistry*; Holmberg, K., Shah, D. O.; Schwuger, M. J., Eds.; Wiley: Chichester, 2002; *Vol.1*; pp 421.
(13) Campanelli, A. R.; Scaramuzza, L. *Acta Crystallogr., Sect. C* **1986**, *C42*, 1380.
(14) Romsted, L. S. Rate Enhancements in Micellar Systems. Ph.D. Thesis, Indiana University, Bloomington, IN, 1975.
(15) Benrraou, M.; Bales, B. L.; Zana, R. *J. Phys. Chem. B* **2003**, *107*, 13432.
(16) Zana, R.; Benrraou, M.; Bales, B. L. *J. Phys. Chem. B* **2004**, *108*, 18195.
(17) Menger, F. M.; Keiper, J. S. *Angew. Chem., Int. Ed. Engl.* **2000**, *39*, 1906.
(18) Menger, F. M.; Keiper, J.; Mbadugha, B. N. A.; Caran, K. L.; Romsted, L. S. *Langmuir* **2000**, *16*, 9095.

(19) Menger, F. M.; Zhang, H.; Caran, K. L.; Seredyuk, V. A.; Apkarian, R. P. *J. Am. Chem. Soc.* **2002**, *124*, 1140.
(20) Geng, Y.; Romsted, L. S.; Menger, F. M. *J. Am. Chem. Soc.* **2006**, *128*, 492.
(21) Ryhänen, S. J.; Säily, V. M. J.; Parry, M. J.; Luciani, P.; Mancini, G.; Alakoskela, J.-M. I.; Kinnunen, P. K. J. *J. Am. Chem. Soc.* **2006**, *128*, 8659.
(22) Fielden, M. L.; Perrin, C.; Kremer, A.; Bergsma, M.; Stuart, M. C.; Camilleri, P.; Engberts, J. B. F. N. *Eur. J. Biochem.* **2001**, *268*, 1269.
(23) Oda, R.; Huc, I.; Schmutz, M.; Candau, S. J.; MacKintosh, F. C. *Nature* **1999**, *399*, 566.
(24) Gronert, S. *Chem. Rev.* **2001**, *101*, 329.
(25) Uggerud, E. *Chem.—Eur. J.* **2006**, *12*, 1127.
(26) Laerdahl, J. K.; Uggerud, E. *Int. J. Mass Spectrom.* **2002**, *214*, 277.
(27) Gronert, S. *J. Mass Spectrom.* **1999**, *34*, 787.
(28) Gronert, S. *Acc. Chem. Res.* **2003**, *36*, 848.
(29) Gronert, S. *J. Am. Chem. Soc.* **1996**, *118*, 3525.
(30) Gronert, S.; Azebu, J. *Org. Lett.* **1999**, *1*, 503.
(31) DePuy, C. H.; Gronert, S.; Mullin, A.; Bierbaum, V. M. *J. Am. Chem. Soc.* **1990**, *112*, 8650.
(32) Gronert, S.; DePuy, C. H.; Bierbaum, V. M. *J. Am. Chem. Soc.* **1991**, *113*, 4009.
(33) Veith, H. J. *Mass Spectrom. Rev.* **1983**, *2*, 419.
(34) Dang, T. A.; Day, R. J.; Hercules, D. M. *Anal. Chem.* **1984**, *56*, 866.
(35) Calas, M.; Cordina, G.; Gilles, I.; Aubagnac, J. L. *J. Mass Spectrom.* **1997**, *32*, 147.
(36) Aubagnac, J. L.; Gilles, I.; Calas, M.; Cordina, G.; Piquet, G.; Portefaix, P.; Giral, L. J. *J. Mass Spectrom.* **1995**, *30*, 985.
(37) Pashynska, V. A.; Kosevich, M. V.; Van den Heuvel, H.; Claeys, M. *Rapid Commun. Mass Spectrom.* **2006**, *20*, 755.
(38) Anslyn, E. V.; Dougherty, D. A. *Modern Physical Organic Chemistry*, 1st ed.; University Science Books: Sausalito, CA, 2006.
(39) Lowry, T. H.; Richardson, K. S. *Mechanism and Theory in Organic Chemistry*, 3rd ed.; Harper and Row: New York, 1987.
(40) Gross, D. S.; Williams, E. R. *Int. J. Mass Spectrom. Ion Processes* **1996**, *157—158*, 305.
(41) McLuckey, S. A. *J. Am. Soc. Mass Spectrom.* **1992**, *3*, 599.
(42) McLafferty, F. W.; Kornfeld, R.; Haddon, W. F.; Leysen, K.; Sakai, I.; Bente, I., P. F.; Tsai, S.-C.; Schuddemage, H. D. R. *J. Am. Chem. Soc.* **1973**, *95*, 3886.
(43) Olmstead, W. N.; Brauman, J. I. *J. Am. Chem. Soc.* **1977**, *99*, 4219.
(44) Oda, R.; Huc, I.; Candau, S. J. *Chem. Commun.* **1997**, 2105.
(45) Gabelica, V.; Karas, M.; De Pauw, E. *Anal. Chem.* **2003**, *75*, 5152.
(46) Goeringer, D. E.; McLuckey, S. A. *J. Chem. Phys.* **1996**, *104*, 2214.
(47) Gronert, S. *J. Am. Soc. Mass Spectrom.* **1998**, *9*, 845.
(48) Lopez, L. L.; Triller, P. R.; Senko, M. W.; Schwartz, J. C. *Rapid Commun. Mass Spectrom.* **1999**, *13*, 663.
(49) Kurimoto, A.; Daikoku, S.; Mutsuga, S.; Kainie, O. *Anal. Chem.* **2006**, *78*, 3461.
(50) David, W. M.; Brodbelt, J. S. *J. Am. Soc. Mass Spec.* **2003**, *14*, 383.
(51) Frisch, M. J.; Trucks, G. W.; Schlegel, H. B.; Scuseria, G. E.; Robb, M. A.; Cheeseman, J. R.; Montgomery, J. A. J.; Vreven, T.; Kudin, K. N.; Burant, J. C.; Millam, J. M.; Iyengar, S. S.; Tomasi, J.; Barone, V.; Mennucci, B.; Cossi, M.; Scalmani, G.; Rega, N.; Petersson, G. A.; Nakatsuji, H.; Hada, M.; Ehara, M.; Toyota, K.; Fukuda, R.; Hasegawa, J.; Ishida, M.; Nakajima, T.; Honda, Y.; Kitao, O.; Nakai, H.; Klene, M.; Li, X.; Knox, J. E.; Hratchian, H. P.; Cross, J. B.; Adamo, C.; Jaramillo, J.; Gomperts, R.; Stratmann, R. E.; Yazyev, O.; Austin, A. J.; Cammi, R.; Pomelli, C.; Ochterski, J. W.; Ayala, P. Y.; Morokuma, K.; Voth, G. A.; Salvador, P.; Dannenberg, J. J.; Zakrzewski, V. G.; Dapprich, S.; Daniels, A. D.; Strain, M. C.; Farkas, O.; Malick, D. K.; Rabuck, A. D.; Raghavachari, K.; Foresman, J. B.; Ortiz, J. V.; Cui, Q.; Baboul, A. G.; Clifford, S.; Cioslowski, J.; Stefanov, B. B.; Liu, G.; Liashenko, A.; Piskorz, P.; Komaromi, I.; Martin, R. L.; Fox, D. J.; Keith, T.; Al-Laham, M. A.; Peng, C. Y.; Nanayakkara, A.; Challacombe, M.; Gill, P. M. W.; Johnson, B.; Chen, W.; Wong, M. W.; Gonzalez, C.; Pople, J. A. *Gaussian 03*, revision B.02; Gaussian, Inc.: Pittsburgh, PA 2003.
(52) Becke, A. D. *J. Chem. Phys.* **1993**, *98*, 1372.
(53) Miehlich, B.; Savin, A.; Stoll, H.; Puress, H. *Chem. Phys. Lett.* **1989**, *157*, 785.
(54) Lee, C.; Yang, W.; Parr, R. G. *Phys. Rev. B: Condens. Matter* **1988**, *37*, 785.
(55) Hay, P. J.; Wadt, W. R. *J. Chem. Phys.* **1985**, *82*, 270.
(56) Glukhovtsev, M. N.; Pross, A.; McGrath, M. P.; Radom, L. *J. Chem. Phys.* **1995**, *103*, 1878.
(57) Boys, S. F.; Bernardi, F. *Mol. Phys.* **1970**, *19*, 553.
(58) Parker, A. J. *Chem. Rev.* **1969**, *69*, 1.
(59) Carroll, F. A. *Perspectives on Structure and Mechanism in Organic Chemistry*; Brooks/Cole: Pacific Grove, CA, 1998.
(60) Gronert, S.; Fong, L.-M. *Aust. J. Chem.* **2003**, *56*, 379.
(61) Gronert, S.; Pratt, L. M.; Mogali, S. *J. Am. Chem. Soc.* **2001**, *123*, 3081.
(62) Gronert, S. *J. Am. Chem. Soc.* **1991**, *113*, 6041.
(63) Bickelhaupt, F. M.; Baerends, E. J.; Nico, S.; Nibbering, M. M.; Zieglerg, T. *J. Am. Chem. Soc.* **1993**, *115*, 9161.

(64) Reaction with F^- gives the longest the C···H bond in the transition structure (Table 5B), and the developing negative charge on carbon would be the most stabilized by the adjacent cationic ammonium group.

JP802801R